Demonstration of Real-time RS-coded DMT wireless Transmission at W-Band Based on FPGA

Jian Chen
National Mobile Communications Research Laboratory
Southeast University
Nanjing, China
jian_chen@seu.edu.cn

Bingchang Hua*
Pervaise Communication Research Center
Purple Mountain Laboratories
Nanjing, China
huabingchang@pmlabs.com.cn

Jiao Zhang
National Mobile Communications Research Laboratory
Southeast University
Nanjing, China
jiaozhang@seu.edu.cn

Junhao Zhang
National Mobile Communications Research Laboratory
Southeast University
Nanjing, China
zhang_junhao@seu.edu.cn

Mingzheng Lei
Pervaise Communication Research Center
Purple Mountain Laboratories
Nanjing, China
leimingzheng@pmlabs.com.cn

Yuancheng Cai
Pervaise Communication Research Center
Purple Mountain Laboratories
Nanjing, China
caiyuancheng@pmlabs.com.cn

Guo Zhao
Science and Technology Management Department Laboratory
Nanjing Wasin Fujikura Optical Communication LTD
Nanjing, China
guo_zhao@nwf.cn

Min Zhu*
National Mobile Communications Research Laboratory
Southeast University
Nanjing, China
minzhu@seu.edu.cn

***Abstract*—We successfully demonstrated a real-time error-free RS-coded DMT transmission system with a net data rate of 4.8Gbit/s at W-band over a 1-m wireless distance. The system performance of different carrier frequencies is also verified.**

Keywords—discrete multi-tone (DMT), Real-time, Reed-Solomon (RS) coding, W-band, FPGA

I. Introduction

With the rapid growth of high data rate services such as the Internet of Things and mobile Internet, higher capacity wireless transmission has become a more urgent goal. Compared with other wireless frequency bands, W-band has rich spectrum resources and lower atmospheric transmission loss, which can meet higher data transmission requirements [1]. However, due to the inherent properties of electronic devices, it is not easy to directly modulate W-band radio signals using pure electrical components on optical carriers [2]. Fortunately, the scheme of optical heterodyne beating is a relatively simple and attractive solution to break through the electronic bandwidth bottleneck[3].

As is well known, discrete multi-tone (DMT) technology has been widely used in optical fiber wireless systems because of its high-frequency spectral efficiency (SE) and excellent robustness against inter-symbol interference (ISI). However, most of the research on DMT technology is based on offline systems. In addition, to improve transmission performance, Reed-Solomon (RS) coding is widely used in wireless and optical fiber systems because of its strong ability to correct bursts and random errors [4]. In [5], the BER performance of real-time DMT transmission system over 25.26 km standard single-mode fiber (SSMF) is significantly improved by using RS coding. In [6], a real-time 2.3Gb/s wavelength division multiplexing(WDM)-based 2×2 Multiple-Input Multiple-Output (MIMO) RS-coded orthogonal frequency division multiplexing(OFDM)-radio over fiber (RoF) system at X-band is successfully demonstrated. However, the signal carrier frequency of the above research is low. Further, a twin single-side-band OFDM transmission scheme at W-band is proposed [7]. In this scheme, only the coarse synchronization and the blind carrier recovery are implemented in the real-time field programmable gate array (FPGA) platform. Therefore, the scheme is only a semi-real-time scheme.

In this paper, we experimentally demonstrate a real-time photonics-aided DMT transmission system based on FPGA at W-band. The 0.7/1.4-Gbaud 16QAM signal are successfully transmitted over 1-m wireless distance. And to research the impact of RS coding with different overheads on the system, two RS coding with coding overheads of 14.3% and 21.4% are applied in the real-time DMT system. Therefore, the maximum net data rate of the system is $1.4 \times 4 \times (1 - 14.3\%) = 4.8$Gbit/s. In addition, we investigated system performance at different carrier frequencies. The experimental results show that error-free transmission can be achieved under different carrier frequencies and coding overhead.

II. Experimental Setup

The experimental setup of the FPGA-enabled real-time DMT wireless system over 0.1/1-m wireless distance at the W band is illustrated in Fig. 1. Fig. 1(d) is the photograph of the real-time DMT wireless transmission system. The digital signal processing (DSP) flowchart for generating the DMT signal based on FPGA is shown in Fig. 1(b). Firstly, the pseudo-random binary sequences(PRBS) are generated by MATLAB, and then RS coding is realized. Two RS coding with coding overhead of 14.3% and 21.4% are implemented in the transmitter. And then, the encoded symbols are mapped with 16-QAM symbols. To achieve a real-valued discrete Fourier transformation (DFT) output, the input vector for the inverse discrete Fourier transform (IDFT) should have complex-conjugate symmetry, i.e., HS. Then, the traditional IDFT method is used to convert the parallel frequency domain signal with a length of 1024 into the time domain signal. To reduce ISI, 32 points used as a cyclic prefix are inserted at the beginning of each OFDM symbol. Then, after the parallel signal in the time domain is converted into a serial signal, the training sequence is added to the front of the OFDM signal for synchronization and channel estimation. In this letter, the OFDM frame consists of one 60-sample synchronization pattern, four TSs, and 56 data-carrying OFDM symbols.

This work was partially supported by National Natural Science Foundation of China (62201397, 62271135, 62101121, 62201393, 62101126).

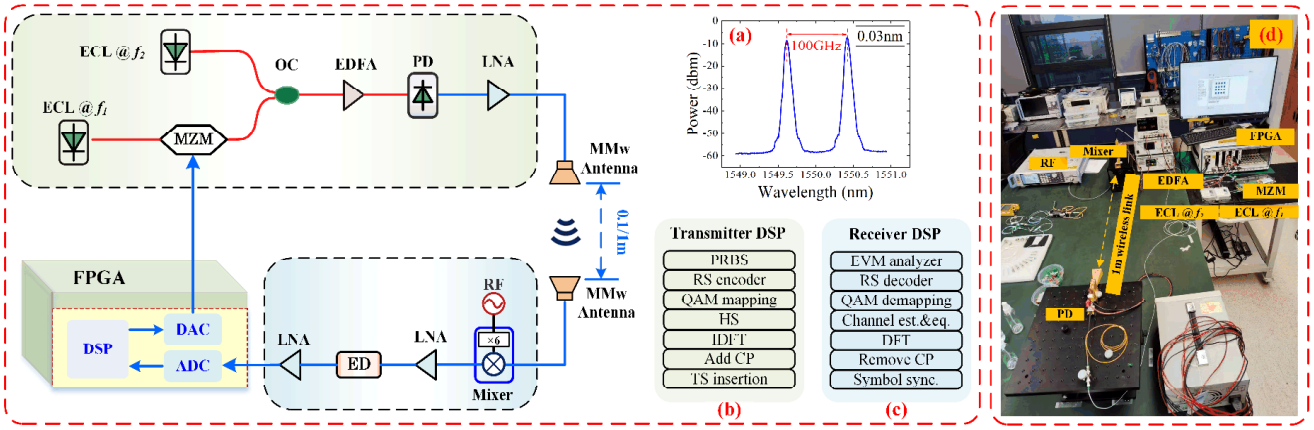

Fig.1. Experimental setup of real-time DMT wireless transmission system. (a) the DSP flowchart of transmitter (b) the DSP flowchart of receiver (c) photograph of the real-time DMT transmission demonstration.

In the experimental setup, a 12-dBm continuous wave (CW) at 1549.62nm emitted from first narrow linewidth free-running tunable external cavity laser (ECL1) is injected into a Mach-Zehnder modulator (MZM). The OFDM symbols driving the MZM are generated by transmitter FPGA module, and converted into analog domain by a 3.2-GSa/s digital to analog converter (DAC) with 12-bit quantization. The other free-running tunable ECL-2 is operated as an optical local oscillator (LO), which has a linewidth of less than 100 kHz. Then optical baseband signal and an optical LO are coupled by an optical coupler (OC). An erbium doped fiber amplifier (EDFA) is used for optical signal boosting amplification before launching into the photodiode (PD). The PD is applied for the 0.1-THz wireless signal generation via heterodyne beating. As shown in Fig.1(a), the RF signal generated after optical heterodyne is a 100-GHz W-band signal by setting the frequency interval of two optical carriers to be about 100-GHz. The W-band wireless signals from PD are amplified by a 35-dB gain low-noise amplifier (LNA1). Finally, the W-band wireless signal can be transmitted to free space via an antenna. After 0.1/1-m wireless transmission, The W-band wireless signal is received by an antenna. Then, the received wireless signal is driven by an RF-integrated harmonic mixer (IHM) to implement electric down conversion. The IHM consists of a mixer and a ×6 frequency multiplier chain, which is driven by an input electronic RF source set to 85 GHz with 0-dBm power. Therefore, a 15-GHz IF signal can be obtained after the RF heterodyne is realized. Then, the IF signal is amplified by an LNA2 to drive the envelope detector (ED) with 500 MHz bandwidth for down-conversion. Finally, the baseband signal is amplified by the LNA3 and then captured by a 3.2-Gs/s analog to digital converter (ADC) for real-time reception and processing.

The 15-GHz IF signal received by ADC is finally processed by real-time receiver DSP based on FPGA. The specific process is shown in Fig.1(c). First, the timing synchronization module is used to determine the starting position of DFT symbols, so as to achieve accurate data reception. Next, the CP with 32 sample lengths is removed, and then 1024 DFT operations are performed. To reduce the impact of channel noise, channel estimation is realized by using four TSs. Then, QAM de-mapping and RS decoding are performed on the signal. Finally, due to the bit error rate is basically zero, the system's performance can be more clearly demonstrated by real-time calculation of EVM and SNR.

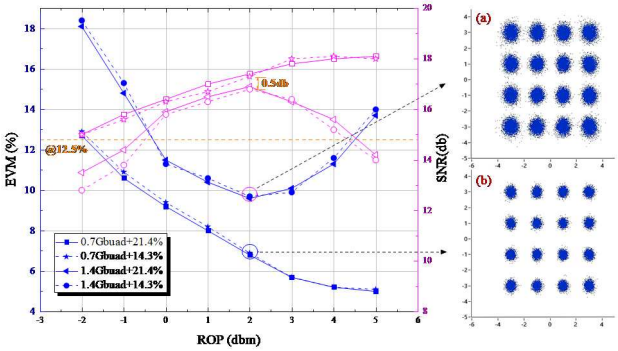

Fig. 2. EVM & SNR curves versus ROP for real-time 0.1-m wireless transmission with 0.7/1.4-Gbuad bandwidth and 14.3% / 21.4% coding overheads. (a) the constellations diagrams in case of 1.4-Gbaud bandwidth (b) the constellations diagrams in case of 0.7-Gbaud bandwidth

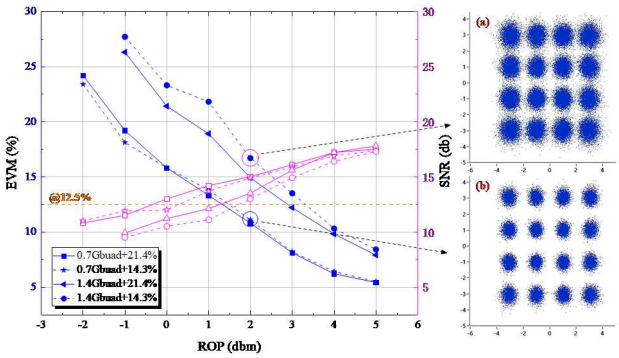

Fig. 3. EVM & SNR curves versus ROP for real-time 1-m wireless transmission with 0.7/1.4-Gbuad bandwidth and 14.3% / 21.4% coding overheads. (a) the constellations diagrams in case of 1.4-Gbuad bandwidth (b) the constellations diagrams in case of 0.7-Gbuad bandwidth

III. Results And Discussions

Fig. 2 shows the EVM and SNR performances versus received optical power (ROP) on a 0.1-m wireless link. In the case of 0.7-Gbaud bandwidth, when the ROP exceeds -1.8-dBm, DMT transmission can achieve EVM below the 3GPP standard limit of 12.5 %. As we can see, when the ROP exceeds 2-dBm, the BER performance starts to deteriorate under the 1.4-Gbaud bandwidth. This is mainly result in system performance degradation due to power saturation of the optoelectronic devices, such as the PD, LNA, EDFA and so on. Moreover, when the ROP is set to 2-dBm, only 0.5-dB SNR penalty can be observed, with the bandwidth expanding

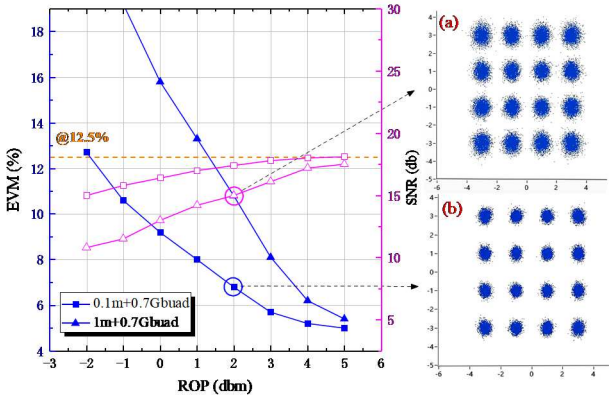

Fig. 4. EVM & SNR curves versus ROP for real-time 0.1/1-m wireless distance with 0.7-Gbaud bandwidth and 21.4% coding overheads. (a) the constellations-diagram in case of 1-m wireless distance (b) the constellations-diagram in case of 0.1-m wireless distance.

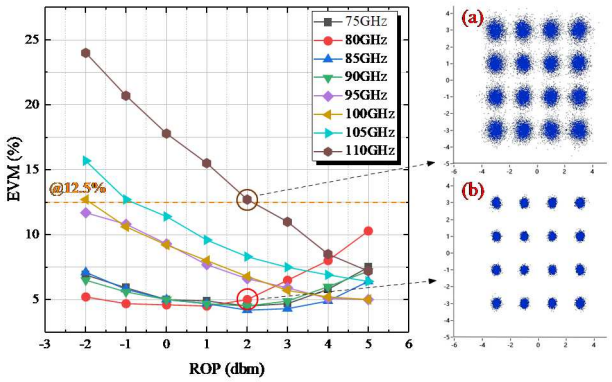

Fig.5. For real-time 0.1-m wireless transmission with 0.7-Gbaud bandwidth and 21.4% coding overheads, EVM curves versus ROP under different transmission frequencies. (a) the constellations diagrams in case of 110-GHz transmission frequency (b) the constellations diagrams in case of 80-GHz transmission frequency.

from 0.7-Gbaud to 1.4-Gbaud. In addition, it can be seen that RS codes with coding overheads of 14.3% and 21.4% have similar EVM performance, which is mainly due to low rate transmission. Fig. 2(a) and (b) give the constellation diagrams of the 1.4-Gbaud and 0.7-Gbaud 16QAM signals in the case of 0.1-m wireless link and 14.3% coding overheads at the ROP of 2-dBm, respectively. The constellation points of the two diagrams are also closely and orderly scattered around the desired points, proving a good wireless communication quality.

Fig.3 shows the EVM and SNR performances versus ROP on a 1-m wireless link. In the case of 1m wireless transmission, the calculated EVMs are better than the 3GPP standard when the ROP is beyond about 3-dBm. When the ROP is 2-dBm and the coding overheads are 14.3%, the EVM and SNR of 0.7-Gbaud bandwidth are reduced by 5.6% and 1.9-dB respectively compared with 1.4-Gbaud bandwidth. Fig. 3(a) and (b) give the constellation diagrams of the 1.4-Gbaud and 0.7-Gbaud 16QAM signals in the case of 1-m wireless link and 14.3% coding overheads at the ROP of 2-dBm, respectively. It can be seen from the constellation diagrams that the signal transmission with higher bandwidth shows poor performance.

We also give the EVM and SNR curves versus ROP of 0.1/1-m wireless transmission distance in Fig. 4. In addition, fig.4 (a) and (b) correspond to the constellation of 1-m wireless transmission and 0.1-m wireless transmission in the case of 21.4% coding overheads and 0.7-Gbaud bandwidth at the ROP of 2-dBm. For 0.1-m wireless distance and 0.7-Gbaud bandwidth case, the EVM meets 12.5% overhead the 3GPP standard limit as long as the ROP is larger than about -2.1-dBm. Whereas in the 1-m wireless distance and 0.7-Gbaud bandwidth case, this value decreases to 1.3-dBm, which exhibits a receiving sensitivity penalty of about 3.3-dB due to the additional 0.9-m wireless delivery. On the other hand, with the increase of ROP, the EVM and SNR in both cases are gradually close. This shows that adjusting transmission power can effectively reduce the impact of different wireless distances.

To further evaluate our real-time DMT wireless transmission system, we test the performance of EVM versus carrier frequency over 0.1-m wireless transmission, as shown in Fig. 5. We fix the signals bandwidth at 0.7-Gbaud. We can observe that, system performance at all carrier frequencies meets 3GPP standards. When the carrier frequency greater than 95-GHz, the EVM performance improves significantly as the ROP increases, whereas when the carrier frequency less than 95-GHz, the EVM performance first increases and then decreases with the increase of ROP. The EVM performance begins to deteriorate over 2-dBm when the carrier frequency less than 95-GHz due to the fact that the power of PD is saturated.

IV. Conclusion

We have experimentally demonstrated a real-time error-free RS-coded DMT W-band photonics-assisted DMT wireless transmission scheme based on FPGA at W-band. The real-time measured EVM and SNR performances showed that the RS-coded DMT signal with a net data rate of 4.8-Gbit/s at W-band is successfully transmitted over 1-m wireless distance. Simultaneously, we compare real-time DMT wireless transmission system performance at various coding overheads and carrier frequencies. The results show that system performance is similar for two RS-codes coding overheads. In addition, as the carrier frequency increases, system performance degrades.

V. References

[1] L. Deng, X. Pang, X. Zhang, et al., “Fiber wireless transmission of 8.3-Gb/s/ch QPSK-OFDM signals in 75–110-GHz band,” IEEE Photonics Technology Letters, vol. 24, no. 5, pp. 383-385, March 2012.

[2] J. Yu, “Photonics-assisted millimeter-wave wireless communication,” IEEE Journal of Quantum Electronics, vol. 53, no. 6, pp. 1–17, December 2017.

[3] X. Li, Y. Xu, J. Xiao, and J. Yu, “W-band millimeter-wave vector signal generation based on precoding-assisted random photonic frequency tripling scheme enabled by phase modulator,” IEEE Photonics Journal, vol. 8, no. 2, pp. 1–10, April 2016.

[4] L. Song, M.-L. Yu, and M. S. Shaffer, “10- and 40-Gb/s forward error correction devices for optical communications,” IEEE Journal of Solid-State Circuits, vol. 37, no. 11, pp. 1565–1573, November 2002.

[5] Y. Shao, Y. Long, A. Wang, et al., "Research on Optical 32QAM-OFDM-PON Access Scheme with Different Numbers of Sub-Carriers Using DMT Modulation," Journal of the European Optical Society, vol. 16, no. 1, pp. 1–5, May 2020.

[6] M. Chen, X. Xiao, J. Yu, X. Li, and F. Li, “Real-Time Gigabit RS-Coded OFDM Signal Transmission over WDM-Based X-Band 2×2 MIMO RoF System,” in Proc. OFC, Los Angeles, March 2017, pp. 1–3.

[7] R. Deng, J. Yu, J. He, et al., “Twin-SSB-OFDM Transmission Over Heterodyne W-Band Fiber-Wireless System With Real-Time Implementable Blind Carrier Recovery,” Journal of Lightwave Technology, vol. 36, no. 23, pp. 5562-5572, December 2018.